Combining the discrete variable representation with the S-matrix Kohn method for quantum reactive scattering

Gerrit C. Groenenboom[a)]
Department of Chemistry, University of California and Chemical Sciences Division, Lawrence Berkeley Laboratory, Berkeley, California 94702

Daniel T. Colbert[b)]
Department of Chemistry, University of California and Chemical Sciences Division, Lawrence Berkeley Laboratory, Berkeley, California 94702 and Department of Chemistry, University of Houston, Houston, Texas, 77204-5641

(Received 26 July 1993; accepted 9 September 1993)

In order to reduce the memory requirements of quantum reactive scattering calculations based on delocalized basis sets, we use a discrete basis in a single interaction region coordinate system, resulting in a sparse Hamiltonian matrix. The resulting set of linear equations is solved via an iterative method which exploits their sparsity. Other important features of our formalism are the use of a truncated grid and distorted waves used to shrink the interaction region, and therefore the basis size. We demonstrate the method and assess its efficiency for the reaction $D+H_2 \rightarrow DH+H$, at a total energy of 0.9 eV and zero total angular momentum ($J=0$).

I. INTRODUCTION

In recent years, methods using square-integrable ($\mathscr{L}^2$) basis functions have been successfully applied to quantum reactive scattering calculations of several three-atom systems. A feature common to these methods, whether based on the S-matrix version of the Kohn variational principle (SKVP)[1-5] or on the (Generalized) Newton variational principle,[6] is the construction of the Hamiltonian matrix in an $\mathscr{L}^2$ interaction region basis set and the subsequent solution of a large set of linear equations. The present paper is based on the SKVP (also a log derivative version of the Kohn variational principle exists[7]). Usually, a direct method (LU-decomposition[8]) is used to solve the linear equations. This requires storage of the Hamiltonian matrix in the fast memory of the computer (if one stores the matrix on disk then the paging cost becomes great), which becomes a bottleneck for problems that require larger basis sets. Alternatively, *iterative* methods can be used to solve the linear equations. Such methods only require the Hamiltonian in operator form, i.e., as a subroutine to perform the matrix-vector multiplication, $\mathbf{y}=\mathbf{H}\mathbf{x}$. It has been pointed out that iterative methods will be particularly beneficial in the case of sparse Hamiltonian matrices, which arise from discrete representations,[9] because then the cost of the matrix-vector multiplication is much less than the N^2 scaling (where N is the number of basis functions) in the case where $\mathbf{H}$ is full. In the SKVP method, the wave function is written as a linear combination of the asymptotic part of the wave function, expressed in Jacobi coordinates of the asymptotic arrangements, and of the $\mathscr{L}^2$ functions, which are set in the exchange, or interaction region. In Miller's formulation,[10] the $\mathscr{L}^2$ functions are defined as a multicentered expansion in the Jacobi coordinates of all arrangements simultaneously, giving rise to a nondirect product basis. However, for discrete representations it is much more convenient to use a single interaction region coordinate system. The latter approach has been demonstrated to work very well for collinear reactive scattering by Colbert and Miller (CM).[9] Here we will demonstrate that it is also suitable for the three-dimensional case.

Once the fundamental memory limitation problem has been solved, the most important task is to improve the performance of the method. For this purpose CM used a truncated grid. In this paper we will show how the matrix-vector multiplication can be implemented to work with great efficiency for such truncated grids. Furthermore, distorted waves have been used to reduce the extent of the interaction region, and thus the number of $\mathscr{L}^2$ basis functions. We show how to construct distorted waves with the following very useful features: (1) they solve the Schrödinger equation exactly (i.e., to arbitrary accuracy) outside the interaction region and (2) they are regular and no cutoff function is needed, as was required in previous implementations of the SKVP. Finally, we present a projection technique which reduces the number of iterations needed to solve the linear equations by eliminating certain unnecessary high energy components in the discrete basis.

Usually, the discrete variable representation (DVR) is derived starting with a delocalized ($\mathscr{L}^2$) basis set, followed by quadrature approximation with the number of quadrature points being equal to the number of basis functions, and finally a specific unitary transformation is applied which diagonalizes the potential energy matrix. However, we prefer to apply the unitary transformation to the delocalized basis, before the quadrature approximation is introduced, resulting in a localized ($\mathscr{L}^2$) basis. Then, upon introducing the quadrature approximation, each quadrature (or grid) point becomes associated with a localized basis function (see Section IV). This interpretation of the DVR has some advantages: (1) it allows us to unify the conventional DVR (based on orthogonal polynomials)

a)Present address: Institute of Theoretical Chemistry, University of Nijmegen, Toernooiveld, 6525 ED Nijmegen, The Netherlands.
b)Present address: Department of Chemistry, Rice University, Houston, Texas 77251.

and the infinite order (or sinc-) DVR introduced by Colbert and Miller[9] and (2) it simplifies the implementation of symmetry (see Section VI).

The resulting formalism can be looked upon as a hybrid method, where the reactive and nonreactive parts of the problem are treated separately. The SKVP formalism puts the reactive part of the calculation on the same footing as a bound-state calculation. Thus, the success of the DVR for bound-state problems motivates our choice of the DVR for the reactive part of the problem. The nonreactive part of the problem, the distorted wave calculation, is almost identical to an inelastic scattering calculation, and it is treated using a propagation method. Note that our method for constructing distorted waves is not linked to the use of a discrete representation, i.e. it could also be used in combination with a "conventional" SKVP calculation using a delocalized basis set.

II. THEORY

The method we describe here may be applied to any bimolecular reaction. We restrict our discussion to a three-atom system, A+BC, with zero total angular momentum and assume all nuclei to be distinguishable. Extensions to $J>0$ and to larger systems are straightforward, although computationally costly. In Sec. VI we will address the issue of indistinguishable nuclei.

A. The triatomic Hamiltonian ($J=0$)

We use Jacobi (or scattering) coordinates $\mathbf{q}_\alpha = (R_\alpha, r_\alpha, z_\alpha)$, where $R_\alpha = |\vec{R}_\alpha|$, $r = |\vec{r}_\alpha|$, and $z_\alpha = \vec{R}_\alpha \cdot \vec{r}_\alpha / (R_\alpha r_\alpha)$ with $\alpha = 1$, 2, and 3 corresponding respectively to the arrangements A+BC, B+AC, and C+AB. Thus, for example, R_1 is the distance from A to the center of mass of the BC fragment and r_1 is the vibrational coordinate for the diatom BC, etc. The volume element for integration $d\tau_\alpha$ is given by

$$d\tau_\alpha = R_\alpha^2 r_\alpha^2 dR_\alpha dr_\alpha dz_\alpha, \tag{1}$$

and the ranges of integration are $[0,\infty]$ for R_α and r_α and $[-1,1]$ for z_α.

The $J=0$ triatomic Hamiltonian expressed in Jacobi coordinates of arrangement α is

$$\hat{H} = \hat{T}_{R_\alpha} + \frac{\hat{j}^2}{2\mu_\alpha R_\alpha^2} + \hat{H}_\alpha^{(0)}(r_\alpha, z_\alpha) + \Delta V_\alpha(\mathbf{q}_\alpha). \tag{2}$$

The first term is the radial part of the relative kinetic energy of the two fragments:

$$\hat{T}_{R_\alpha} = -\frac{\hbar^2}{2\mu_\alpha} \frac{1}{R_\alpha} \frac{\partial^2}{\partial R_\alpha^2} R_\alpha. \tag{3}$$

The second term in Eq. (2) is the corresponding angular part, where we have used the fact that for $J=0$ the orbital angular momentum of the atom about the diatom ($\hat{l}^2$) is equal to the rotational angular momentum of the diatom ($\hat{j}^2$). The third term is the diatomic Hamiltonian:

$$\hat{H}_\alpha^{(0)}(r_\alpha, z_\alpha) = -\frac{\hbar^2}{2m_\alpha} \frac{1}{r_\alpha} \frac{\partial^2}{\partial r_\alpha^2} r_\alpha + \frac{\hat{j}^2}{2m_\alpha r_\alpha^2} + V_\alpha^r(r_\alpha), \tag{4}$$

where $V_\alpha^r(r_\alpha)$ is the diatomic potential. The last term in Eq. (2) is the interaction potential for which we have

$$\lim_{R_\alpha \to \infty} \Delta V_\alpha(R_\alpha, r_\alpha, z_\alpha) = 0, \tag{5}$$

where $\Delta V_\alpha + V_\alpha^r$ is the full potential. The reduced masses in these equations are, for arrangement 1:

$$1/\mu_1 = 1/m_A + 1/(m_B + m_C), \tag{6}$$

$$1/m_1 = 1/m_B + 1/m_C, \tag{7}$$

and similarly for arrangements 2 and 3.

We now introduce the channel eigenfunctions, $\Phi_\mathbf{n}$, of each arrangement, defined as the eigenfunctions of $\hat{H}_\alpha^{(0)}$, with eigenvalues $\epsilon_\mathbf{n}$:

$$[\hat{H}_\alpha^{(0)}(r_\alpha, z_\alpha) - \epsilon_\mathbf{n}] \Phi_\mathbf{n}(r_\alpha, z_\alpha) = 0. \tag{8}$$

Here $\mathbf{n} \equiv (\alpha, v, j)$ denotes the arrangement and the vibrational and rotational quantum numbers. The functions $\Phi_\mathbf{n}$ for which $\epsilon_\mathbf{n} < E$ (E being the total scattering energy) are the open channels, the remainder being closed channels. The channel eigenfunctions are separable into rotational and vibrational parts:

$$\Phi_\mathbf{n}(r_\alpha, z_\alpha) = \bar{P}_j(z_\alpha) \phi_\mathbf{n}^{\mathrm{vib}}(r_\alpha)/r_\alpha. \tag{9}$$

The $\bar{P}_j$ are normalized Legendre polynomials, which are the eigenfunctions of $\hat{j}^2$:

$$\hat{j}^2 \bar{P}_j(z) = \hbar^2 j(j+1) \bar{P}_j(z). \tag{10}$$

The second factor in Eq. (9) are the solutions of the radial Schrödinger equation for the diatom:

$$\left[-\frac{\hbar^2}{2\mu_\alpha} \frac{\partial^2}{\partial r_\alpha^2} + \frac{\hbar^2 j(j+1)}{2\mu_\alpha r_\alpha^2} + V_\alpha^r(r_\alpha) - \epsilon_\mathbf{n} \right] \phi_\mathbf{n}^{\mathrm{vib}}(r_\alpha) = 0. \tag{11}$$

For each arrangement we can now write down the asymptotic form of the Schrödinger equation by subtracting the interaction potential [Eq. (5)] from the total Hamiltonian [Eq. (2)]:

$$[\hat{H} - \Delta V_\alpha(\mathbf{q}_\alpha) - E] \Psi_\mathbf{n}(\mathbf{q}_\alpha) = 0. \tag{12}$$

This equation can be separated into a part depending on the scattering coordinate and a part depending on the other coordinates yielding

$$\Psi_\mathbf{n}(R_\alpha, r_\alpha, z_\alpha) = R_\alpha^{-1} u_\mathbf{n}(R_\alpha) \Phi_\mathbf{n}(r_\alpha, z_\alpha), \tag{13}$$

where $u_\mathbf{n}$ is a solution of the radial equation:

$$\left[\frac{\partial^2}{\partial R_\alpha^2} + k_\mathbf{n}^2 - \frac{j(j+1)}{R_\alpha^2} \right] u_\mathbf{n}(R_\alpha) = 0 \tag{14}$$

and $k_\mathbf{n}^2 = 2\mu_\alpha(E - \epsilon_\mathbf{n})/\hbar^2$. Note that for now we are only interested in the open channels, so $k_\mathbf{n}$ is real (and positive). The regular solutions of Eq. (14) are

$$J_\mathbf{n}(R_\alpha) = x\hat{j}_j(x) v_\mathbf{n}^{-1/2} \tag{15}$$

and the irregular solutions are

$$Y_\mathbf{n}(R_\alpha) = x\hat{y}_j(x) v_\mathbf{n}^{-1/2}, \tag{16}$$

with $x=|k_n|R_\alpha$ and $v_n=\hbar|k_n|/\mu_\alpha$. Here $\hat{j}_j(x)$ and $\hat{y}_j(x)$ are spherical Bessel functions of the first kind and the third kind, respectively.[11,12]

From these two sets of real functions we can construct complex functions with incoming $(-)$ or outgoing $(+)$ boundary conditions:

$$H_n^{(\pm)}(R_\alpha)=J_n(R_\alpha)\pm iY_n(R_\alpha). \tag{17}$$

The normalization $(v_n^{-1/2})$ was chosen such that the radial flux is unity. Also, note that $(H^{(-)})^*=H^{(+)}$.

The closed channels ($k_n^2<0$) are obtained by setting $x=+i|k_n|R_\alpha$ in Eqs. (15) and (16).

B. The S-matrix version of the Kohn variational principle

We solve the time-independent Schrödinger equation using the S-matrix version of the Kohn variational principle. The SKVP (at total energy E) can be written as

$$\mathbf{S}_{n,n'}=\text{ext}\left[\tilde{\mathbf{S}}_{n,n'}+\frac{i}{\hbar}\langle\tilde{\psi}_n|\hat{H}-E|\tilde{\psi}_{n'}\rangle\right]. \tag{18}$$

Here $\tilde{\mathbf{S}}$ is the S matrix corresponding to the trial wave functions $\tilde{\psi}_n$. By "ext" we mean that we need a stationary point of the expression with respect to first order variations in $\tilde{\psi}_n$.

The crucial step in any variational calculation is choosing a suitable trial wave function. In the present context, it can be written as

$$\tilde{\psi}_n=\tilde{\psi}_n^{\text{bound}}+\tilde{\psi}_n^{\text{free}}. \tag{19}$$

This form of the trial wave function emphasizes the hybrid nature of the present approach, discussed in the Introduction. In a variational calculation, one has enormous freedom in constructing the trial wave function; the above form of $\tilde{\psi}$ introduces a separation which allows the profitable use of widely disparate computational methods in the same calculation. In particular, we will construct $\tilde{\psi}^{\text{free}}$ using a propagation method, and $\tilde{\psi}^{\text{bound}}$ *via* a basis set expansion in the DVR. The "bound" part of the function is a linear combination of $\mathcal{L}^2$ basis functions, Υ_k:

$$\tilde{\psi}_n^{\text{bound}}(\vec{x})=\sum_{k=1}^{N}\Upsilon_k(\vec{x})c_{k,n}. \tag{20}$$

It is important to note that the basis functions (and thus, $\tilde{\psi}^{\text{bound}}$) may may be expressed in *whatever coordinates,* $\vec{x}$, are most convenient. In the examples in this paper we will use the Jacobi coordinates of arrangement 1. However, we have successfully used other coordinate systems with which to expand $\tilde{\psi}^{\text{bound}}$, including Jacobi coordinates of the other arrangements, Radau coordinates,[13] valence (also called bond-angle) coordinates, and normal coordinates of the transition state.

The "free" part of the trial wave function is

$$\tilde{\psi}_n^{\text{free}}(\mathbf{q}_\alpha)=-\chi_n(\mathbf{q}_\alpha)+\sum_{n'}\chi_{n'}^*(\mathbf{q}_{\alpha'})\tilde{\mathbf{S}}_{n',n}, \tag{21}$$

where the functions χ_n must be regular at $R_\alpha=0$ and asymptotically ($R_\alpha\to\infty$) must have incoming wave boundary conditions:

$$\chi_n(\mathbf{q}_\alpha)\sim R_\alpha^{-1}H_n^{(-)}(R_\alpha)\Phi_n(r_\alpha,z_\alpha). \tag{22}$$

To give some insight into the role of the "bound" and the "free" parts of the trial wave function we consider the case where the interaction potential has a finite range, i.e., $\Delta V_\alpha(\mathbf{q}_\alpha)=0$ for $R_\alpha>R_\alpha^{\max}$. Taking $H+H_2$ as a typical example, we find that this is a very good approximation if we take $R_\alpha^{\max}\approx 10$ Bohr. We will now call the region where $R_\alpha<R_\alpha^{\max}$ (for $\alpha=1$, 2 or 3) the interaction region and the rest the asymptotic region. We could construct the free part of the trial wave function by taking

$$\chi_n(\mathbf{q}_\alpha)=R_\alpha^{-1}f(R_\alpha)H_n^{(-)}(R_\alpha)\Phi_n(r_\alpha,z_\alpha), \tag{23}$$

where $f(R_\alpha)$ is a cutoff function[2] that regularizes χ_n at $R_\alpha=0$, i.e., $f(0)=0$ and switches on smoothly to $f(R_\alpha)=1$ for all $R_\alpha\geqslant R^{\max}$. This way the free functions form a complete basis for the asymptotic regions and bound functions only have to be placed in the interaction region. Formally, this basis will only be complete if the closed channels are included, giving rise to an augmented S matrix (see, e.g., Ref. 7). Alternatively, one can leave out the closed channels and converge the calculation with respect to the size of the interaction region. We use the latter approach. Substituting the trial wave function [Eqs. (19), (20), and (21)] into the variational expression [Eq. (18)] yields the following expression for the S matrix:[2,4]

$$\mathbf{S}=\frac{i}{\hbar}[\mathbf{B}-\mathbf{C}^T\cdot(\mathbf{B}^*)^{-1}\cdot\mathbf{C}], \tag{24}$$

where

$$\mathbf{B}=\mathbf{M}_{0,0}-\mathbf{M}_0^T\cdot\mathbf{M}^{-1}\cdot\mathbf{M}_0, \tag{25}$$

$$\mathbf{C}=\mathbf{M}_{1,0}-\mathbf{M}_0^\dagger\cdot\mathbf{M}^{-1}\cdot\mathbf{M}_0, \tag{26}$$

and

$$(\mathbf{M}_{0,0})_{n,n'}=\langle\chi_n|\hat{H}-E|\chi_{n'}\rangle, \tag{27}$$

$$(\mathbf{M}_{1,0})_{n,n'}=\langle\chi_n^*|\hat{H}-E|\chi_{n'}\rangle, \tag{28}$$

$$(\mathbf{M}_0)_{k,n}=\langle\Upsilon_k|\hat{H}-E|\chi_n\rangle, \tag{29}$$

$$\mathbf{M}_{k,k'}=\langle\Upsilon_k|\hat{H}-E|\Upsilon_{k'}\rangle. \tag{30}$$

Here n runs over all open channels and all arrangements and $k,k'=1,\ldots,N$, where N is the total number of $\mathcal{L}^2$ basis functions. Note that here we have defined the bra, $\langle|$, without the usual complex conjugation.

If we take a real $\mathcal{L}^2$ basis, $\mathbf{M}$ (the bound–bound matrix) will be a real symmetric matrix. $\mathbf{M}_0$ (the bound–free matrix) is complex rectangular and the number of columns is equal to the total number of open channels.

III. COMPUTATIONAL STRATEGY

Since N, the number of $\mathcal{L}^2$ basis functions, is typically much larger than the total number of open channels, the computational bottleneck is the solution of the linear system

$$\mathbf{M}\cdot\mathbf{x}=\mathbf{M}_0 \tag{31}$$

in order to calculate $\mathbf{M}^{-1}\mathbf{M}_0$ in Eqs. (25) and (26). An important feature of the SKVP is that it puts quantum scattering calculations on the same footing as eigenvalue, or bound state, problems. Thus, we may borrow from the wealth of methods developed over the years for such problems. One successful approach to eigenvalue problems has been the use of contracted basis sets in order to minimize N. Alternatively, one can use a discrete representation of the Hamiltonian in combination with an iterative method to solve the linear equations. The latter is the approach we are currently investigating.

In a DVR the basis functions are associated with grid points in configuration space.[14] In a multidimensional problem the grid can be constructed as a direct product of one-dimensional grids, if a single interaction region coordinate system is being used, as was done by Colbert and Miller.[9] Since the proposal of Miller in 1969[10] to treat exchange in time-independent reactive scattering calculations by using a multicentered expansion of the wave functions (i.e., use basis functions simultaneously in Jacobi coordinates of all arrangements), this idea has been implemented in several computational frameworks, including SKVP.[4] Attempts to adapt the DVR to this approach have lead to a nonsparse $\mathbf{M}$ matrix,[15] however. Therefore, following CM, we depart from the multicentered expansion, and construct our DVR in a single global coordinate system.

In a discrete representation any multiplicative operator (such as the potential energy operator in the position representation) will be diagonal. This makes it particularly efficient to multiply the $\mathbf{M}$ matrix into a vector, which makes the use of iterative methods to solve Eq. (31) practical (multiplication with kinetic energy terms can be done efficiently by exploiting their direct product structure, see Section IV C). Since the $\mathbf{M}$ matrix is indefinite (it has both positive and negative eigenvalues) we use the SYMMLQ algorithm[16] to solve the linear system of Eq. (31). The SYMMLQ algorithm uses Lanczos recursions to construct a Gram–Schmidt orthogonalized basis in the Krylov space $\{\mathbf{b},\mathbf{Mb},\mathbf{M}^2\mathbf{b},\ldots\}$, where $\mathbf{b}$ is the right-hand side of the linear equations. In this basis the linear system is tridiagonal and can be easily solved using LQ decomposition. The algorithm is implemented in such a way that at every iteration the LQ decomposition and the solution are updated. The advantage of an iterative method is that one only needs to store a few vectors of length N, instead of the whole ($N\times N$) $\mathbf{M}$ matrix. As a result, the method becomes cpu-bound, rather than memory-bound.

Although storage of $\mathbf{M}$ is no longer a problem, it is still important to keep N, the number of grid points, as low as possible, because both the cost per iteration and the number of iterations needed to converge Eq. (31) depend on N. Currently, we reduce N in three ways.

(1) We truncate the grid by discarding all points where the potential energy is above some cutoff energy (V^{cut}), an idea already exploited in two-dimensional calculations by Colbert and Miller.[9] The implicit physical assumption is that the wave function will have nearly zero amplitude in these regions. This results in V^{cut} becoming a convergence parameter.

(2) We exploit symmetry. We cannot use the threefold symmetry in the H_3 system because the Jacobi coordinates break the symmetry. However, it is relatively easy to use twofold symmetry in Jacobi coordinates. For example, in the $D+H_2$ system we exploit all the symmetry.

(3) In Section II B we already showed that we only place $\mathcal{L}^2$ basis functions in the interaction region. For a discrete representation that means that we only keep points for which $R_\alpha < R_\alpha^{\max}$, $\alpha=1,\ldots,3$, as was done before.[9] Now the idea is to minimize $R_\alpha^{\max}$ by using *inelastically distorted waves* as free functions, as described in Section V.

The number of iterations required to solve Eq. (31) is sometimes considerable (we found cases with n_{iter} on the order of N). It turns out to be possible to reduce the number of iterations by projecting out high angular momentum components of the grid, without appreciably affecting the solution. Appendix A describes the projection technique in some detail. This technique is very close to the spirit of Friesner's pseudospectral method.[17] In our examples the number of iterations was reduced by roughly 50% because of the smaller condition number (i.e., the ratio between the smallest and the largest eigenvalue) of $\mathbf{M}$. After taking into account the overhead of the projection (which must be done twice at each iteration) this still results in a speedup of about 40%.

IV. DISCRETE VARIABLE REPRESENTATION

A. General background

The routine use of the discrete variable representation (DVR) in molecular dynamics calculations has already been seen a decade go (Ref. 18), though its origins are almost 30 years old.[19] During this time, there have been various extensions and reformulations of the basic idea. Many have been based on the connection made by Dickinson and Certain[20] between the discrete representation that diagonalizes the potential energy matrix, and Gaussian quadrature points and weights. We redefine the DVR in order to unify the DVR based on Gaussian quadratures with the DVR introduced by Colbert and Miller.[9] The latter DVR (which we use for radial coordinates) yields an equally spaced grid which is particularly convenient in scattering calculations, since it does not depend on some equilibrium structure.

We start by discussing a one-dimensional problem; the generalization to the multidimensional case will be given in the next section. The DVR can be introduced in several ways. We find the following definition to be most convenient:

A DVR consists of an orthonormal basis set

$$\{\phi_i(x),\ i=1,...,n\} \tag{32}$$

and a n-point quadrature with the points and weights

$$\{(x_k,w_k),\ k=1,...,n\} \tag{33}$$

and the property

$$\phi_i(x_k)=w_k^{-1/2}\delta_{ik}, \tag{34}$$

together with the rule that the potential energy matrix (and all other multiplicative operators) are computed within the quadrature approximation. Note that the number of quadrature points, n, is equal to the number of basis functions. We will call the functions ϕ_i DVR functions.

Using this approximation it can be easily shown that the potential energy matrix becomes diagonal:

$$\begin{aligned} \mathbf{V}_{ij}&=\langle\phi_i|\hat{V}|\phi_j\rangle \\ &\approx \sum_{k=1}^{n} w_k\,\phi_i(x_k)V(x_k)\phi_j(x_k) \\ &= \sum_{k=1}^{n}\delta_{ik}V(x_k)\delta_{jk}=V(x_i)\delta_{ij}. \end{aligned} \tag{35}$$

Using the theory of orthogonal polynomials and Gaussian integration we can construct a DVR.[20] For example, consider a set of normalized Hermite polynomials

$$h_i(x)=w(x)^{1/2}N_{i-1}H_{i-1}(x),\quad i=1,...,n, \tag{36}$$

where we have absorbed the square root of the weight function $[w(x)^{1/2}]$ into the functions h_i, and N_i is the normalization[12] (i.e., the functions h_i are harmonic oscillator eigenfunctions). The n-point Gauss–Hermite quadrature will be exact for the overlap matrix

$$\langle h_i|h_j\rangle=\sum_{k=1}^{n} w_k h_i(x_k)h_j(x_k)=\delta_{ij}, \tag{37}$$

where w_k are the so-called adjusted quadrature weights, i.e., $w_k = w_k' w(x_k)^{-1/2}$ and w_k' are the normal Gauss–Hermite quadrature weights. From this equation it follows that the matrix

$$U_{ki}=w_k^{1/2}h_i(x_k) \tag{38}$$

is unitary and thus the set

$$\phi_k(x)=\sum_{i=1}^{n} U_{ki}h_i(x),\quad k=1,...,n \tag{39}$$

satisfies Eq. (34), since

$$\phi_k(x_j)=\sum_{i=1}^{n} U_{ki}h_i(x_j) \tag{40}$$

$$=w_k^{-1/2}\sum_{i=1}^{n} U_{ki}U_{ji}=w_k^{-1/2}\delta_{kj}. \tag{41}$$

B. Sinc-function DVR

A DVR does not *have* to be derived from orthogonal polynomials. Consider the following set of functions:

$$\phi_n(x)=\Delta^{-1/2}\,\mathrm{sinc}\left[\pi\left(\frac{x}{\Delta}-n\right)\right],\quad n=-\infty,...,+\infty \tag{42}$$

[$\mathrm{sinc}(x)\equiv\sin(x)/x$] together with the quadrature $\{(x_n,w_n)=(n\Delta,\Delta),\ n=-\infty,...,+\infty\}$. These functions clearly satisfy Eq. (34). The properties of this set of functions can be understood most easily by realizing that they are the Fourier transforms of a Fourier basis in momentum-space, i.e.,

$$\phi_n(x)=(2\pi)^{-1/2}\int_{-\infty}^{+\infty} e^{-ipx}\tilde{\phi}_n(p)dp, \tag{43}$$

where

$$\tilde{\phi}_n(p)=\begin{cases}(2p_{\max})^{-1/2}e^{in\pi(p/p_{\max})}, & |p|\leqslant p_{\max}\\ 0, \quad \text{otherwise}\end{cases} \tag{44}$$

and $p_{\max}=\pi/\Delta$. From this it immediately follows that $\{\phi_n(x),\ n=-\infty,...,+\infty\}$ is an orthogonal basis set, that spans all functions that have a highest momentum component $p\leqslant p_{\max}$. This also means that the quadrature, which is exact for the overlap matrix, will be exact for any function with a highest frequency component $2p_{\max}$.

The matrix elements for the first and second derivative operators can be evaluated analytically for these sinc functions. These formulas have been given before[9,21] but we will reproduce them here

$$\left\langle\phi_n\left|\frac{\partial}{\partial x}\right|\phi_m\right\rangle=\begin{cases}0, & n=m,\\ \dfrac{1}{\Delta}\dfrac{(-1)^{n-m}}{(n-m)}, & n\neq m,\end{cases} \tag{45}$$

and

$$\left\langle\phi_n\left|\frac{\partial^2}{\partial x^2}\right|\phi_m\right\rangle=\begin{cases}-\dfrac{1}{3}\dfrac{\pi^2}{\Delta^2}, & n=m,\\ -\dfrac{2}{\Delta^2}\dfrac{(-1)^{n-m}}{(n-m)^2}, & n\neq m.\end{cases} \tag{46}$$

These matrix elements can also be evaluated using the quadrature. This gives the same result, since the quadrature is exact for the overlap of sinc functions (ϕ_n) and taking the derivative of a sinc function does not introduce higher frequency components.

For radial coordinates ($r\in[0,\infty]$) we can use the following set:

$$\phi_n^-(r)=\phi_n(r)-\phi_n(-r),\quad n=1,...,\infty, \tag{47}$$

which we will call "wrapped" sinc functions. These functions are orthonormal on the range $[0,\infty]$ and they satisfy Eq. (34) if we use the quadrature $\{(r_n,w_n)=(n\Delta,\Delta),\ n=1,...,\infty\}$. For the wrapped functions we have

$$\left\langle\phi_n^-\left|\frac{\partial^2}{\partial r^2}\right|\phi_m^-\right\rangle$$

$$=\begin{cases}-\dfrac{1}{3}\dfrac{\pi^2}{\Delta^2}-\dfrac{2}{\Delta^2}\dfrac{(-1)^{n+m}}{(n+m)^2}, & n=m,\\ -\dfrac{2}{\Delta^2}\left[\dfrac{(-1)^{n-m}}{(n-m)^2}+\dfrac{(-1)^{n+m}}{(n+m)^2}\right], & n\neq m.\end{cases} \tag{48}$$

In practice we will of course truncate the sets, which is equivalent to assuming that the function that is being represented is zero outside a certain range of the coordinate.

C. Multidimensional case

The generalization of the DVR to more than one dimension is straightforward. One simply uses the direct product of one-dimensional DVRs. The only complication arises from the truncation of the multidimensional grid. Here, we will give the formalism for a general three-dimensional interaction region coordinate system $\vec{x} = (x,y,z)$. For some bound–free matrix elements one has to deal with two coordinate systems, so it will be most convenient to keep the volume element of integration [the Jacobian $J(\vec{x})$] explicitly in the formalism. For the scalar product between two real functions $f(\vec{x})$ and $g(\vec{x})$ we have

$$\langle f|g\rangle \equiv \int\int\int J(\vec{x}) f(\vec{x}) g(\vec{x}) d\vec{x}. \tag{49}$$

The ranges of integration depend on the type of coordinate. We assume that for every coordinate we have a quadrature $\{(x_i,w_i^x),\ i=1,\ldots,n_x\}$ (and similarly for y and z). Thus, for a grid point with the indices $\mathbf{p}=(i,j,k)$ we have

$$\vec{x}_\mathbf{p} \equiv (x_i,y_j,z_k). \tag{50}$$

Associated with each grid point we have a quadrature weight

$$w_\mathbf{p} = w_i^x w_j^y w_k^z \tag{51}$$

and a DVR function

$$\Upsilon_\mathbf{p}(\vec{x}) = J(\vec{x})^{-1/2} \phi_i^x(x) \phi_j^y(y) \phi_k^z(z) \tag{52}$$

with the property

$$\Upsilon_\mathbf{p}(\vec{x}_{\mathbf{p}'}) = [w_\mathbf{p} J(\vec{x}_\mathbf{p})]^{-1/2} \delta_{ii'} \delta_{jj'} \delta_{kk'}. \tag{53}$$

This direct product grid of $n_x \times n_y \times n_z$ points should cover the entire interaction region. We truncate this grid by using the criteria given in Section III.

The **M**-matrix elements are defined by

$$M_{\mathbf{p}\mathbf{p}'} = \langle \Upsilon_\mathbf{p}|\hat{H}-E|\Upsilon_{\mathbf{p}'}\rangle \tag{54}$$

$$= \int\int\int J(\vec{x}) \Upsilon_\mathbf{p}(\vec{x}) (\hat{H}-E) \Upsilon_{\mathbf{p}'}(\vec{x}) d\vec{x}. \tag{55}$$

For multiplicative terms in $\hat{H}$ we get only diagonal terms again (within the quadrature approximation of course):

$$\langle \Upsilon_\mathbf{p}| V(\vec{x}) |\Upsilon_{\mathbf{p}'}\rangle = V(\vec{x}_\mathbf{p}) \delta_{ii'} \delta_{jj'} \delta_{kk'}. \tag{56}$$

For kinetic energy terms of the form

$$\hat{T}_x = J(\vec{x})^{-1/2} \hat{T}'_x J(\vec{x})^{1/2}, \tag{57}$$

like, e.g., the radial kinetic energy operator of Eq. (3), we get

$$\langle \Upsilon_\mathbf{p}| \hat{T}_x |\Upsilon_{\mathbf{p}'}\rangle = (\hat{T}'_x)_{ii'} \delta_{jj'} \delta_{kk'}, \tag{58}$$

where

$$(\hat{T}'_x)_{ii'} = \int \phi_i(x) \hat{T}'_x \phi_{i'}(x) dx. \tag{59}$$

For kinetic energy terms with a coordinate-dependent prefactor, or in general for any product of operators, we insert the resolution of identity in the DVR basis

$$\hat{I} \approx \sum_{i=1}^{N} |\Upsilon_i\rangle\langle\Upsilon_i| \tag{60}$$

between the factors and use the quadrature approximation for the multiplicative terms. For example,

$$\langle \Upsilon_\mathbf{p}| f(x,y) \hat{T}_z |\Upsilon_{\mathbf{p}'}\rangle = \delta_{ii'} \delta_{jj'} f(x_i,y_j) (\hat{T}'_z)_{kk'}. \tag{61}$$

We also compute the $\mathbf{M}_0$-matrix elements using the quadrature approximation. From Eq. (29) we have

$$(\mathbf{M}_0)_{\mathbf{p},\mathbf{n}} = \langle \Upsilon_\mathbf{p}|\hat{H}-E|\chi_\mathbf{n}\rangle \tag{62}$$

$$\approx [w_\mathbf{p} J(\vec{x}_\mathbf{p})]^{1/2} [(\hat{H}-E)\chi_\mathbf{n}]_{\vec{x}=\vec{x}_\mathbf{p}}. \tag{63}$$

D. Implementation

In order to solve Eq. (31) with an iterative method we need to implement the matrix-vector multiplication:

$$\mathbf{d} = \mathbf{M} \cdot \mathbf{c}, \tag{64}$$

where the components $d_\mathbf{p}$ and $c_\mathbf{p}$ of the vectors **d** and **c** correspond to the grid point with the indices (i,j,k). We will discuss the implementation for the various terms in **M** separately.

Potential energy terms are diagonal, so we can store them in a one-dimensional array of length N. Operating a diagonal operator on a vector is done in a single loop.

The structure of a kinetic energy term depends on the ordering of the grid points. For example, if the x index (i) is running fastest, the $\hat{T}_x$ operator [Eq. (58)] will be block diagonal. The sizes of the diagonal blocks will vary depending on the number of grid points in each "row" of the grid (i.e., after truncation of the grid). So for the $\hat{T}_x$ operator we just need to store one square matrix of dimension n_x from which we can "clip" all the differently sized diagonal blocks. Of course we must also store the lowest and the highest x index of each row in the grid, which tells us what part of this matrix we need.

A problem arises when the truncation of the grid cuts a row into two (or more) pieces. We solve this problem by treating each piece as if it were a separate row, so that we have a diagonal block in $\hat{T}_x$ for each row of consecutive points in the grid. This means that we set the kinetic energy matrix elements that connect points on opposite sides of a "gap" to zero. This procedure is consistent with the approximation inherent in the truncation of the grid. As discussed before, eliminating grid points is equivalent to assuming the potential to be infinite in that region, and the coupling across such a region can thus be set to zero. Note that there can still be indirect kinetic coupling *around* such a region. If the physical assumption is poor, meaning that the wave function has appreciable amplitude in that region, one simply must not truncate there. We checked to make sure that this approximation does not affect the answer.

However, we warn that kinetic energy operators of the form $\partial^2/\partial x\partial y$ will no longer be symmetric (or, in general, Hermitian) when we make this approximation for both factors $\partial/\partial x$ and $\partial/\partial y$ separately. This problem can be overcome by working with the symmetrized form $(1/2)\{(\partial^2/\partial x\partial y)+(\partial^2/\partial y\partial x)\}$ instead.

The implementation of the $\hat{T}_y$ operator is seemingly much more difficult. Of course, if the grid points were ordered with the y index (j) running fastest we could use the same implementation we just described for the $\hat{T}_x$ operator. This observation is the key to the algorithm that we propose: before applying $\hat{T}_y$ we *reorder* the vector $\mathbf{c}$ and before we add the result to $\mathbf{d}$ we apply the inverse permutation. The permutation is stored in an integer array of length N, and the reordering can be done in a single loop of length N. The cost of finding the permutation is negligible since it only needs to be done once, instead of every iteration. Furthermore, it can be done with a general purpose sorting routine.[22] For example, for the y ordering, the sorting criterion is point ($\mathbf{p}$) must come after point ($\mathbf{p}'$) if

$$z_k > z_{k'} \text{ or}$$
$$\{z_k = z_{k'} \text{ and } [x_k > x_{k'} \text{ or } (x_k = x_{k'} \text{ and } y_j > y_{j'})]\}. \tag{65}$$

As such, we can exploit the sparsity and the truncation in a straightforward manner by this sorting procedure.

V. DISTORTED WAVES

We have already discussed the flexibility one has in choosing the $\mathscr{L}^2$ basis (here, a DVR). This is, however, only a part of the basis that forms the variational wave function; one also has considerable freedom in constructing the free waves $\chi_{\mathbf{n}}$. The only requirements on them is that they satisfy the boundary conditions at $R_\alpha=0$ and $R_\alpha=\infty$, and that they solve the Schrödinger equation from $R_\alpha=\infty$ inward to $R_\alpha=R_\alpha^{\max}$, the outer boundary of the interaction region. Zhang and Miller[4,5] previously proposed using "distorted" waves that solve the Schrödinger equation from $R_\alpha=\infty$ inward to a much smaller value of $R_\alpha^{\max}$ than do simple spherical waves, for example. We follow this strategy, but our implementation of the idea differs sufficiently from their proposal to warrant discussion.

Suppose we solve the equation

$$[\hat{H}-E+V_\alpha^{(1)}(\mathbf{q}_\alpha)]\chi_{\mathbf{n}}^{(1)}(\mathbf{q}_\alpha)=0, \tag{66}$$

where $V_\alpha^{(1)}$ is some additional potential energy term. Then in all regions where $V_\alpha^{(1)}(\mathbf{q}_\alpha)=0$, the functions $\chi_{\mathbf{n}}^{(1)}(\mathbf{q}_\alpha)$ will solve the original Schrödinger equation. Of course if we take $V_\alpha^{(1)}$ to be zero everywhere we are back to the reactive scattering problem we started with. The idea, following that of Baer and co-workers,[23,24] is to take a short range repulsive potential that separates arrangements from one another by turning Eq. (66) into an inelastic scattering problem. To better reflect the purpose of this potential we prefer to call it a *barrier* potential, rather than distortion potential. When we use the functions $\chi_{\mathbf{n}}^{(1)}$ as distorted waves we do not need a cutoff function, since these inelastic scattering wave functions are regular at $R_\alpha=0$. In other words, the barrier potential takes the role of the cutoff function. However, these inelastic wave functions do not satisfy incoming wave boundary conditions, as required. To construct functions with the desired asymptotic behavior we could use the irregular solutions of Eq. (66), but in that case we would need a cutoff function again. Instead, we determine the regular solutions of another inelastic problem with a slightly different barrier potential, $V_\alpha^{(2)}$, and take the correct linear combination of the two sets of solutions. One of the advantages of this approach is that we can use well established methods to solve the inelastic problem. We chose the renormalized Numerov method of Johnson,[25,26] rather than a Log-derivative method, since the former allows for an easy calculation of the wave functions. In the computation of the free–free and bound–free integrals we will assume the inelastic solutions to be well converged. This means that we must include closed channels in the propagation, which prevents us from using a simple method like the normal Numerov propagation. At the same time, however, the possibility to include closed channels in the computation of the distorted waves allows us to reduce the size of the interaction region even further.

To simplify the formalism, we choose barrier potentials dependent on R_α only, although this is not a strict requirement. Also, we make sure that the distorted waves of different arrangements do not overlap, so that we do not have to compute free–free integrals involving different arrangements. Now we will show how to determine the correct linear combination of the two sets of functions.

The two inelastic problems for arrangement α are defined by

$$[\hat{H}-E+V_\alpha^{(p)}(R_\alpha)]\chi_{\mathbf{n}}^{(p)}(\mathbf{q}_\alpha)=0, \quad p=1,2. \tag{67}$$

The solution is written as

$$\chi_{\mathbf{n}}^{(p)}(\mathbf{q}_\alpha)=\sum_{\mathbf{n}'}\Phi_{\mathbf{n}'}(r_\alpha,z_\alpha)\mathbf{U}_{\mathbf{n}',\mathbf{n}}^{(p)}(R_\alpha)/R_\alpha, \tag{68}$$

Here $\mathbf{n}$ runs over only the open channels but $\mathbf{n}'$ involves both open and closed channels. Note that since we are only concerned with one arrangement at a time, $\mathbf{n}'\equiv(\alpha,v',j')$. The expansion leads to the coupled channel equations for $\mathbf{U}^{(p)}$:

$$\frac{\partial^2}{\partial R_\alpha^2}\mathbf{U}^{(p)}(R_\alpha)=\mathbf{W}^{(p)}(R_\alpha)\mathbf{U}^{(p)}(R_\alpha), \tag{69}$$

where

$$\mathbf{W}_{\mathbf{n},\mathbf{n}'}^{(p)}(R_\alpha)=\left[-k_{\mathbf{n}}^2+\frac{j(j+1)}{R_\alpha^2}\right]\delta_{\mathbf{n},\mathbf{n}'}+\frac{2\mu_\alpha}{\hbar^2}\mathbf{V}_{\mathbf{n},\mathbf{n}'}^{(p)}(R_\alpha) \tag{70}$$

with

$$\mathbf{V}_{\mathbf{n},\mathbf{n}'}^{(p)}(R_\alpha)=\langle\Phi_{\mathbf{n}}(r_\alpha,z_\alpha)\,|\,V_\alpha^{(p)}(R_\alpha)+\Delta V_\alpha(R_\alpha,r_\alpha,z_\alpha)\,|\,\Phi_{\mathbf{n}'}(r_\alpha,z_\alpha)\rangle_{r_\alpha,z_\alpha}. \tag{71}$$

Asymptotically $\mathbf{U}^{(p)}$ can be written as

$$\mathbf{U}^{(p)}(R_\alpha)\sim\mathbf{J}(R_\alpha)+\mathbf{Y}(R_\alpha)\mathbf{K}^{(p)}. \tag{72}$$

In this equation we can take all matrices to be $m\times m$, with m being the number of open channels, since the coefficients for the closed channels can be set to zero asymptotically. $\mathbf{J}$ and $\mathbf{Y}$ are diagonal matrices with the spherical Bessel functions of Eqs. (15) and (16), respectively, on the diagonal.

First we rewrite this solution with S-matrix boundary conditions. From Eq. (17) we have

$$\mathbf{J}(\mathbf{q}_\alpha)=[\mathbf{H}^{(+)}(\mathbf{q}_\alpha)-\mathbf{H}^{(-)}(\mathbf{q}_\alpha)]/2i, \tag{73}$$

$$\mathbf{Y}(\mathbf{q}_\alpha)=[\mathbf{H}^{(+)}(\mathbf{q}_\alpha)+\mathbf{H}^{(-)}(\mathbf{q}_\alpha)]/2, \tag{74}$$

so we can rewrite Eq. (72) as

$$\mathbf{U}^{(p)}(\mathbf{q}_\alpha)\mathbf{A}^{(p)}\sim-\mathbf{H}^{(-)}(\mathbf{q}_\alpha)\mathbf{S}_p^\dagger+\mathbf{H}^{(+)}(\mathbf{q}_\alpha) \tag{75}$$

with

$$\mathbf{A}^{(p)}=2(-i\mathbf{I}+\mathbf{K}^{(p)})^{-1}, \tag{76}$$

$$\mathbf{S}_p^\dagger=(-i\mathbf{I}-\mathbf{K}^{(p)})(-i\mathbf{I}+\mathbf{K}^{(p)})^{-1}. \tag{77}$$

Note that, using the fact that $\mathbf{K}^{(p)}$ is real and symmetric, it is easy to prove that these inverses exist.

Subtracting Eq. (75) with $p=2$ from the same equation with $p=1$ we get

$$\mathbf{U}^{(1)}(\mathbf{q}_\alpha)\mathbf{A}^{(1)}-\mathbf{U}^{(2)}(\mathbf{q}_\alpha)\mathbf{A}^{(2)}\sim\mathbf{H}^{(-)}(\mathbf{q}_\alpha)(\mathbf{S}_2^\dagger-\mathbf{S}_1^\dagger). \tag{78}$$

Defining

$$\Delta=\mathbf{S}_2-\mathbf{S}_1, \tag{79}$$

$$\mathbf{E}^{(1)}=\mathbf{A}^{(1)}(\Delta^\dagger)^{-1}, \tag{80}$$

$$\mathbf{E}^{(2)}=-\mathbf{A}^{(2)}(\Delta^\dagger)^{-1}, \tag{81}$$

we get

$$\mathbf{U}^{(1)}(\mathbf{q}_\alpha)\mathbf{E}^{(1)}+\mathbf{U}^{(2)}(\mathbf{q}_\alpha)\mathbf{E}^{(2)}\sim\mathbf{H}^{(-)}(\mathbf{q}_\alpha). \tag{82}$$

Finally, we can construct distorted waves with incoming wave boundary conditions from the two sets of solutions of Eq. (67):

$$\chi_{\mathbf{n}}(\mathbf{q}_\alpha)=\sum_{p=1}^{2}\sum_{\mathbf{n}'}\chi_{\mathbf{n}'}^{(p)}(\mathbf{q}_\alpha)\mathbf{E}_{\mathbf{n}',\mathbf{n}}^{(p)}, \tag{83}$$

where now $\mathbf{n}$ and $\mathbf{n}'$ run over only the open channels.

Note that a problem arises when Δ is (nearly) singular. This will happen, for example, when the difference between the two distortion potentials goes to zero, since that will make $\mathbf{S}_1$ and $\mathbf{S}_2$ [Eq. (79)] identical. However, it can also happen for other reasons and then it can actually be used to advantage. We will return to this point in Section VIII.

A. Bound–free elements

To compute the $\mathbf{M}_0$-matrix elements we must operate with $\hat{H}-E$ on the incoming waves. Assuming that the inelastic problem has been converged sufficiently well, we can use [from Eq. (67)]

$$(\hat{H}-E)\chi_{\mathbf{n}}^{(p)}=-V_\alpha^{(p)}\chi_{\mathbf{n}}^{(p)} \tag{84}$$

and with Eq. (83) we get

$$(\hat{H}-E)\chi_{\mathbf{n}}=-\sum_{p=1}^{2}V_\alpha^{(p)}\sum_{\mathbf{n}'}\chi_{\mathbf{n}'}^{(p)}\mathbf{E}_{\mathbf{n}',\mathbf{n}}^{(p)}. \tag{85}$$

All that remains to be done is the evaluation of this function at all interaction region grid points. The renormalized Numerov propagation yields the $\mathbf{U}(R_\alpha)$ matrices at a grid, i.e., we have (dropping the arrangement labels)

$$\mathbf{U}_i^{(p)}\equiv\mathbf{U}^{(p)}(R_i),\quad R_i=ih,\quad i=n_0,n_0+1,\ldots,n_1, \tag{86}$$

where h is a grid spacing. This grid will in general not coincide with the interaction region grid. Thus in order to evaluate Eq. (68) at some interaction region grid point (R,r,z) (still dropping the arrangement labels), we must obtain $\mathbf{U}^{(p)}(R)$ by interpolation. Johnson gives a fourth-order interpolation formula for this[25] in the one-dimensional case (i.e., $\mathbf{U}$ being a one-by-one matrix). The generalization of his formula for our multichannel problem is straightforward, but it requires the evaluation and inversion of $\mathbf{W}^{(p)}(R)$ [Eq. (70)] at each interaction region grid point. However, following Johnson, we managed to derive a slightly different fourth-order interpolation formula which only requires the $\mathbf{W}^{(p)}$ matrices (and not their inverses) at the renormalized Numerov grid points

$$\mathbf{W}_i^{(p)}\equiv\mathbf{W}^{(p)}(R_i). \tag{87}$$

These matrices can be stored on a disk file during the computation of the distorted waves. The derivation of our interpolation formula is given in Appendix B; here we just give the result. Assume we want to compute the $\mathbf{U}$ matrix at a grid point R_a which lies between the two propagation grid points R_{i-1} and R_i:

$$R_a=R_{i-1}+ah. \tag{88}$$

Defining

$$b=1-a \tag{89}$$

the interpolation formula, with truncation error of order h^4, is [also dropping the (p) superscript]

$$U(R_a)=bU_{i-1}+aU_i+\frac{ab(a-2)h^2}{6}W_{i-1}U_{i-1}+\frac{ab(b-2)h^2}{6}W_iU_i\ . \tag{90}$$

One final note about the application of this formula: usually it will not be possible to keep all the $\mathbf{U}$ and $\mathbf{W}$ matrices in core memory and in the most unfortunate case, the program will have to read two $\mathbf{U}$ and two $\mathbf{W}$ matrices from disk for every grid point in the interaction region. Thus, it is much more economical to sort the interaction region grid points on increasing value of R before the interpolation is done. This way one will only have to go through the file with the $\mathbf{U}$ matrices and the file with the $\mathbf{W}$ matrices once. Afterward, the $\mathbf{M}_0$ elements can be reordered again.

B. Free–free integrals

The computation of the free–free integrals is also based on Eq. (85):

$$(\mathbf{M}_{0,0})_{\mathbf{n},\mathbf{n}'}=\langle\chi_{\mathbf{n}}|\hat{H}-E|\chi_{\mathbf{n}'}\rangle \tag{91}$$

$$=\sum_{p=1}^{2}\sum_{q=1}^{2}\sum_{\mathbf{m}}\sum_{\mathbf{m}'}\mathbf{E}^{(p)}_{\mathbf{m},\mathbf{n}}\mathbf{E}^{(q)}_{\mathbf{m}',\mathbf{n}'}\mathbf{X}^{(p,q)}_{\mathbf{m},\mathbf{m}'}, \tag{92}$$

where $\mathbf{m}$ and $\mathbf{m}'$ run over the open channels and

$$\mathbf{X}^{(p,q)}_{\mathbf{m},\mathbf{m}'}=-\int_0^\infty dR V_\alpha^{(q)}(R)\sum_{\mathbf{n}}\mathbf{U}^{(p)}_{\mathbf{n},\mathbf{m}}(R)\mathbf{U}^{(q)}_{\mathbf{n},\mathbf{m}'}(R). \tag{93}$$

In this last equation $\mathbf{n}$ runs over all channels. Here we have used the orthogonality of the channel eigenfunctions Φ_n. In our implementation the integral is evaluated by summing over all Numerov grid points and multiplying by the Numerov grid spacing (h). To compute $\mathbf{M}_{1,0}$ we also use Eq. (92), but with $\mathbf{E}^{(p)}_{\mathbf{m},\mathbf{n}}$ replaced by its complex conjugate $[\mathbf{E}^{(p)}_{\mathbf{m},\mathbf{n}}]^*$.

C. Choice of the barrier potentials

The barrier potentials $V^{(p)}(R)$ need to satisfy somewhat contradictory conditions. First they should be strongly repulsive for small R in order to prevent overlap of the incoming waves of different arrangements. This condition can be waived, provided one is willing to compute free–free matrix elements off-diagonal in arrangement index. This could allow further reduction of the interaction region. Furthermore, the barriers need to be placed as far inward as possible, since the size of the interaction region grid is determined by the range of the barriers. These two conditions could be met with a hard wall potential. However, if the barrier switches on too sharply, the incoming waves will change abruptly in a small range, and we will need a high density of grid points in order to obtain accurate bound–free integrals. In other words, the barriers have to be smooth as well. We tried barriers of several analytic forms, and obtained good results with a barrier of the following form:

$$V_\alpha^{(p)}(R)=\begin{cases}a_p(R-R^{\max})^4, & R<R^{\max},\\ 0, & \text{otherwise},\end{cases} \tag{94}$$

where a_p is a constant. The discontinuity in the fourth derivative of this function caused no problems. Furthermore, taking a_2 to be about $1.1\times a_1$ was sufficient to avoid problems with the inversion of Δ in Eqs. (80) and (81).

VI. SYMMETRY

For the SKVP based on the multicentered expansion of the wave function it has been shown before how to exploit the symmetry due to the presence of two or three identical atoms in a three-atom system.[10,4] In the current DVR-SKVP approach we have a single interaction region coordinate system. This means that in the case of two identical atoms we choose (e.g., Jacobi) coordinates of the arrangement associated with the unique atom. For example, in the DH_2 system we use arrangement 1 ($D+H_2$) interaction region coordinates. However, in the case of three identical atoms, such a choice will always break the equivalence between one arrangement and the two others. Of course, upon convergence the symmetry will be restored, but it does mean that we cannot exploit all the symmetry in, e.g., H_3. In the definition of Jacobi coordinates one has the freedom to choose the sign of z_α. Assuming we use arrangement 1 interaction region coordinates, it will be convenient to use a definition of the Jacobi coordinates that is symmetric between arrangement 2 and 3, rather than the "cyclic" one used by Miller.[10,4] Rather than giving the final ($J\geqslant 0$) formulas, we will limit ourselves to the ($J=0$) case, but give the derivation in some detail, which will illuminate how to exploit symmetry in general.

Let $\vec{x}_D$, $\vec{x}_H$, and $\vec{x}_{H'}$ be the space-fixed coordinates of the atoms. Using the notation $x\equiv|\vec{x}|$ and $\hat{x}\equiv\vec{x}/x$, we define the Jacobi coordinates of the three arrangements $\mathbf{q}_\alpha=(R_\alpha,r_\alpha,z_\alpha)$ as

$$\vec{R}_1=\vec{x}_D-(\vec{x}_H+\vec{x}_{H'})/2, \tag{95}$$

$$\vec{R}_2=\vec{x}_H-(m_D\vec{x}_D+m_H\vec{x}_{H'})/(m_D+m_H), \tag{96}$$

$$\vec{R}_3=\vec{x}_{H'}-(m_D\vec{x}_D+m_H\vec{x}_H)/(m_D+m_H), \tag{97}$$

$$\vec{r}_1=\vec{x}_{H'}-\vec{x}_H, \tag{98}$$

$$\vec{r}_2=\vec{x}_D-\vec{x}_{H'}, \tag{99}$$

$$\vec{r}_3=\vec{x}_D-\vec{x}_H, \tag{100}$$

$$z_\alpha=\hat{R}_\alpha\cdot\hat{r}_\alpha,\quad \alpha=1,2,3. \tag{101}$$

The only symmetry operation we will consider here is the permutation of the two hydrogen atoms, $\hat{\mathscr{P}}$, which is defined by

$$\hat{\mathscr{P}}\vec{x}_H=\vec{x}_{H'}. \tag{102}$$

Note that $\hat{\mathscr{P}}^2=I$ and that the $J=0$ Hamiltonian ($\hat{H}$) for DH_2, is invariant under $\hat{\mathscr{P}}$, i.e., $[\hat{\mathscr{P}},\hat{H}]=0$. Thus, in order to exploit symmetry, we construct a trial wave function that is an eigenfunction of $\hat{\mathscr{P}}$.

The transformation properties of the Jacobi coordinates under $\hat{\mathscr{P}}$ can be easily derived from Eqs. (95)–(101):

$$\hat{\mathscr{P}}(\mathbf{q}_1)\equiv\hat{\mathscr{P}}(R_1,r_1,z_1)=(R_1,r_1,-z_1), \tag{103}$$

$$\hat{\mathscr{P}}\mathbf{q}_2=\mathbf{q}_3, \tag{104}$$

$$\hat{\mathscr{P}}\mathbf{q}_3=\mathbf{q}_2. \tag{105}$$

Note that here we have $\hat{\mathscr{P}}z_2=z_3$, while in the cyclic definition of the Jacobi coordinates, one has $\hat{\mathscr{P}}z_2=-z_3$. The effect of $\hat{\mathscr{P}}$ on a general function (f) of arbitrary coordinates ($\mathbf{x}$) is defined by

$$\hat{\mathscr{P}}f(\mathbf{x})\equiv f(\hat{\mathscr{P}}^{-1}\mathbf{x}). \tag{106}$$

Using the property of Legendre polynomials that

$$\bar{P}_j(-z)=(-1)^j\bar{P}_j(z) \tag{107}$$

we can derive, from Eq. (9), that

$$\hat{\mathscr{P}}\Phi_{1,v,j}(r_1,z_1)=(-1)^j\Phi_{1,v,j}(r_1,z_1) \tag{108}$$

and from Eq. (23) or Eq. (83)

$$\hat{\mathscr{P}}\chi_{1,v,j}(\mathbf{q}_1)=(-1)^j\chi_{1,v,j}(\mathbf{q}_1). \tag{109}$$

For arrangements 2 and 3 we find

$$\hat{\mathscr{P}}\chi_{2,v,j}(\mathbf{q}_2)=\chi_{2,v,j}(\mathbf{q}_3), \tag{110}$$

$$\hat{\mathscr{P}}\chi_{3,v,j}(\mathbf{q}_3)=\chi_{3,v,j}(\mathbf{q}_2). \tag{111}$$

Thus we see that the functions $\chi_{1,v,j}$ are eigenfunctions of $\hat{\mathscr{P}}$. For arrangements 2 and 3 we wish to construct symmetrized distorted waves. First we note that we can derive that $\chi_{2,v,j}\equiv\chi_{3,v,j}$, provided that the barrier potentials $V_\alpha^{(p)}$ are the same for the two arrangements [see Eq. (67)]. Thus it can be shown that the functions

$$\chi_{\pm,v,j}=2^{-1/2}[\chi_{2,v,j}(\mathbf{q}_2)\pm\chi_{3,v,j}(\mathbf{q}_3)] \tag{112}$$

are eigenfunctions of $\hat{\mathscr{P}}$. To simplify the formulas we introduce the notation

$$\mathbf{e}=(\alpha=1,v,j=\text{even}), \tag{113}$$

$$\mathbf{o}=(\alpha=1,v,j=\text{odd}), \tag{114}$$

$$\mathbf{b}=(\alpha=2,v,j), \tag{115}$$

$$\mathbf{c}=(\alpha=3,v,j), \tag{116}$$

$$\mathbf{s}=(\alpha=+,v,j), \tag{117}$$

$$\mathbf{a}=(\alpha=-,v,j). \tag{118}$$

Before we can construct symmetrized free waves there is one complication: we must show that the trial **S** matrix has the same symmetry as the exact one [see Eq. (21)]. Of course, this will happen upon convergence. However, for a finite-dimensional calculation we must inspect Eqs. (24)–(30). Here, we will just give an outline of the proof that $\mathbf{S}_{\mathbf{b},\mathbf{b}'}=\mathbf{S}_{\mathbf{c},\mathbf{c}'}$. We start with the first term on the rhs of Eq. (25):

$$(\mathbf{M}_{0,0})_{\mathbf{b},\mathbf{b}'}=\langle\chi_{\mathbf{b}}(\mathbf{q}_2)|\hat{H}-E|\chi_{\mathbf{b}'}(\mathbf{q}_2)\rangle \tag{119}$$

$$=\langle\hat{\mathscr{P}}\chi_{\mathbf{c}}(\mathbf{q}_3)|\hat{H}-E|\hat{\mathscr{P}}\chi_{\mathbf{c}'}(\mathbf{q}_3)\rangle \tag{120}$$

$$=\langle\chi_{\mathbf{c}}(\mathbf{q}_3)|\hat{\mathscr{P}}^\dagger(\hat{H}-E)\hat{\mathscr{P}}|\chi_{\mathbf{c}'}(\mathbf{q}_3)\rangle \tag{121}$$

$$=(\mathbf{M}_{0,0})_{\mathbf{c},\mathbf{c}'}. \tag{122}$$

Here we have used $\hat{\mathscr{P}}^\dagger\hat{\mathscr{P}}=I$, $[\hat{\mathscr{P}},\hat{H}]=0$, and $\chi_{\mathbf{b}}\equiv\chi_{\mathbf{c}}$. The complication arises in the second term in Eq. (25), because there the interaction region $\mathscr{L}^2$ basis enters. We can only prove that

$$(\mathbf{M}_0)_{\mathbf{b}}^T\mathbf{M}^{-1}(\mathbf{M}_0)_{\mathbf{b}'}=(\mathbf{M}_0)_{\mathbf{c}}^T\mathbf{M}^{-1}(\mathbf{M}_0)_{\mathbf{c}'} \tag{123}$$

if the $\mathscr{L}^2$ basis is closed under $\hat{\mathscr{P}}$; i.e., we may write

$$\hat{\mathscr{P}}|\Upsilon_i\rangle=\sum_j|\Upsilon_j\rangle\mathbf{P}_{j,i}, \tag{124}$$

where **P** is the matrix representation of $\hat{\mathscr{P}}$ in the $\mathscr{L}^2$ basis. Using this equation we get

$$\langle\Upsilon_i|\hat{H}-E|\chi_{\mathbf{b}}(\mathbf{q}_2)\rangle=\langle\Upsilon_i|\hat{\mathscr{P}}^\dagger(\hat{H}-E)\hat{\mathscr{P}}|\chi_{\mathbf{b}}(\mathbf{q}_2)\rangle \tag{125}$$

$$=\sum_j\mathbf{P}_{i,j}\langle\Upsilon_j|\hat{H}-E|\chi_{\mathbf{c}}(\mathbf{q}_3)\rangle. \tag{126}$$

Thus, in matrix notation we have

$$(\mathbf{M}_0)_{\mathbf{b}}=\mathbf{P}^\dagger(\mathbf{M}_0)_{\mathbf{c}}. \tag{127}$$

Similarly we can derive for the bound–bound matrix elements

$$\mathbf{M}=\mathbf{P}^\dagger\mathbf{M}\mathbf{P}. \tag{128}$$

Using these two equations and the fact that for a real $\mathscr{L}^2$ basis $\mathbf{P}^T=\mathbf{P}^\dagger$, one can easily derive Eq. (123). Along the same lines we can derive the symmetry properties of the **C** matrix [Eq. (26)] and finally of the **S** matrix [Eq. (24)].

We can summarize the result as follows: the free waves [Eq. (21)] will have the same symmetry properties as the χs if the space spanned by the $\mathscr{L}^2$ basis set is invariant under $\hat{\mathscr{P}}$ and the $\mathscr{L}^2$ basis is real. Thus, finally, we have $\tilde{\psi}_{\mathbf{b}}^{\text{free}}=\tilde{\psi}_{\mathbf{c}}^{\text{free}}$ and we can construct symmetrized free waves

$$\tilde{\psi}_{\pm,v,j}^{\text{free}}=2^{-1/2}[\tilde{\psi}_{\mathbf{b}}^{\text{free}}(\mathbf{q}_2)\pm\tilde{\psi}_{\mathbf{c}}^{\text{free}}(\mathbf{q}_3)]. \tag{129}$$

With this definition of the free waves the relation between the unsymmetrized **S** matrix ($\tilde{\mathbf{S}}$) and the symmetrized **S** matrix (which has diagonal blocks $\tilde{\mathbf{S}}^+$ and $\tilde{\mathbf{S}}^-$) is given by

$$\tilde{\mathbf{S}}_{\mathbf{e},\mathbf{e}}=\tilde{\mathbf{S}}_{\mathbf{e},\mathbf{e}}^+, \tag{130}$$

$$\tilde{\mathbf{S}}_{\mathbf{o},\mathbf{o}}=\tilde{\mathbf{S}}_{\mathbf{o},\mathbf{o}}^-, \tag{131}$$

$$\tilde{\mathbf{S}}_{\mathbf{b},\mathbf{e}}=\tilde{\mathbf{S}}_{\mathbf{c},\mathbf{e}}=2^{-1/2}\tilde{\mathbf{S}}_{\mathbf{s},\mathbf{e}}^+, \tag{132}$$

$$\tilde{\mathbf{S}}_{\mathbf{b},\mathbf{o}}=\tilde{\mathbf{S}}_{\mathbf{c},\mathbf{o}}=2^{-1/2}\tilde{\mathbf{S}}_{\mathbf{a},\mathbf{o}}^-, \tag{133}$$

$$\tilde{\mathbf{S}}_{\mathbf{b},\mathbf{b}}=\tilde{\mathbf{S}}_{\mathbf{c},\mathbf{c}}=\tfrac{1}{2}(\tilde{\mathbf{S}}_{\mathbf{s},\mathbf{s}}^+ +\tilde{\mathbf{S}}_{\mathbf{a},\mathbf{a}}^-), \tag{134}$$

$$\tilde{\mathbf{S}}_{\mathbf{b},\mathbf{c}}=\tfrac{1}{2}(\tilde{\mathbf{S}}_{\mathbf{s},\mathbf{s}}^+ -\tilde{\mathbf{S}}_{\mathbf{a},\mathbf{a}}^-). \tag{135}$$

(One gets the other blocks from $\tilde{\mathbf{S}}=\tilde{\mathbf{S}}^T$.)

Now we give the expression for the **M**-matrix elements in the symmetrized DVR basis. Let $\mathbf{p}=(i,j,k)$ be the indices of an interaction region grid point defined in the Jacobi coordinates of arrangement 1, i.e., $\mathbf{q}_{\mathbf{p}}=(R_i,r_j,z_k)$. Let $\hat{\mathscr{P}}\mathbf{q}_{\mathbf{p}}=(R_i,r_j,-z_k)$ be a grid point that has the indices $\tilde{\mathbf{p}}=(i,j,\tilde{k})$, with $z_{\tilde{k}}=-z_k$. Furthermore, assume that for the DVR functions associated with the grid points we have

$$\hat{\mathscr{P}}\Upsilon_{\mathbf{p}}(\mathbf{q})=\Upsilon_{\tilde{\mathbf{p}}}(\mathbf{q}). \tag{136}$$

Note that these assumptions hold for Gauss–Legendre DVR. The symmetrized DVR basis is defined as

$$\Upsilon_{\mathbf{p}}^{\pm}(\mathbf{q})=2^{-1/2}(I\pm\hat{\mathscr{P}})\Upsilon_{\mathbf{p}}(\mathbf{q}). \tag{137}$$

where **p** runs over all points with $z_k>0$, assuming that we have an even number of Gauss-Legendre points, i.e., there is no grid point with $z_k=0$. (It is possible to use an odd number of Gauss–Legendre points, in which case the DVR function corresponding to the point $z_k=0$ will be even with respect to $\hat{\mathscr{P}}$). For the **M** matrix in the symmetrized basis we find

$$\mathbf{M}_{\mathbf{p},\mathbf{q}}^{\pm}=\langle\Upsilon_{\mathbf{p}}^{\pm}|\hat{H}-E|\Upsilon_{\mathbf{q}}^{\pm}\rangle \tag{138}$$

$$=\mathbf{M}_{\mathbf{p},\mathbf{q}}\pm\mathbf{M}_{\mathbf{p},\tilde{\mathbf{q}}}. \tag{139}$$

For the bound–free elements we have

$$(\mathbf{M}_0^+)_{\mathbf{p},\mathbf{e}}=\langle\Upsilon_{\mathbf{p}}^{\pm}|\hat{H}-E|\chi_{\mathbf{e}}\rangle \tag{140}$$

$$=2^{1/2}(\mathbf{M}_0)_{\mathrm{p,e}}, \tag{141}$$

$$(\mathbf{M}_0^-)_{\mathrm{p,o}}=2^{1/2}(\mathbf{M}_0)_{\mathrm{p,o}}, \tag{142}$$

$$(\mathbf{M}_0^+)_{\mathrm{p,s}}=(\mathbf{M}_0)_{\mathrm{p,b}}+(\mathbf{M}_0)_{\mathrm{p,c}} \tag{143}$$

$$=(\mathbf{M}_0)_{\mathrm{p,b}}. \tag{144}$$

In this last step we used the assumption that the distorted waves of arrangement 3 do not penetrate the region with $z_k<0$. This is equivalent to the assumption that distorted waves of different arrangements do not overlap. Similarly we have

$$(\mathbf{M}_0^-)_{\mathrm{p,a}}=(\mathbf{M}_0)_{\mathrm{p,b}}. \tag{145}$$

For the free–free integrals in the symmetrized basis we find

$$(\mathbf{M}_{0,0}^+)_{\mathrm{e,e}}=(\mathbf{M}_{0,0})_{\mathrm{e,e}}, \tag{146}$$

$$(\mathbf{M}_{0,0}^-)_{\mathrm{o,o}}=(\mathbf{M}_{0,0})_{\mathrm{o,o}}, \tag{147}$$

$$(\mathbf{M}_{0,0}^+)_{\mathrm{s,s}}=(\mathbf{M}_{0,0})_{\mathrm{b,b}}, \tag{148}$$

$$(\mathbf{M}_{0,0}^-)_{\mathrm{a,a}}=(\mathbf{M}_{0,0})_{\mathrm{b,b}}. \tag{149}$$

These equations also hold for $\mathbf{M}_{1,0}$.

VII. APPLICATION TO D+H$_2$

We demonstrate the convergence behavior of the method with respect to the interaction region parameters. We also show the effect of using distorted waves on the number of interaction region points and we give some details about timings. The reaction,

$$\mathrm{D}+\mathrm{H}_2(j,v)\rightarrow\mathrm{DH}(j',v')+\mathrm{H}, \tag{150}$$

in three dimensions, with total angular momentum $J=0$ and total energy $E=0.9$ eV was chosen, since a benchmark calculation of Zhang *et al.* is available.[27] Like Zhang *et al.* we use the Liu–Siegbahn–Truhlar–Horowitz (LSTH) potential energy surface.[28] Symmetry was exploited in our calculation and here we present only results of the symmetric case, i.e., even j. Note that for arrangement 2 (and, because of the symmetry, arrangement 3) this calculation still includes both even and odd j'. This gives 7 open channels for arrangement 1 (D+H$_2$) and 17 for arrangement 2 (DH+H).

First, we summarize the steps in our reactive scattering computation.

1. Calculate the channel eigenfunctions $\{\Phi_n\}$ and eigenvalues $\{\epsilon_n\}$ for H_2 and DH [see Eq. (8)].

2. Construct the distorted waves, $\{\chi_n\}$, for each arrangement by renormalized Numerov propagation (see Section V). Using these, calculate the free–free matrices, $\mathbf{M}_{0,0}$ [Eq. (27)] and $\mathbf{M}_{1,0}$ [Eq. (28)].

3. Construct the truncated interaction-region DVR grid (see Section IV), with or without symmetry.

4. Using the channel functions, distorted waves, and the DVR grid, evaluate the bound–free matrix, $\mathbf{M}_0$ [Eq. (29)], for each arrangement, using Eqs. (140)–(145) in case of symmetry.

TABLE I. Deviation from unitarity of the **P** matrix in % as a function of n_θ and n_B.

n_θ \ n_B	3.0	3.5	4.0	4.5
18	2.9	3.1	3.2	3.2
20	2.5	2.1	2.0	2.1
22	0.49	0.46	0.46	0.49
24	0.30	0.080	0.075	0.076
26	0.11	0.031	0.032	0.028
28	0.15	0.0044	0.0048	0.0036
30	0.14	0.0044	0.0048	0.0011
32	0.13	0.0044	0.0048	−0.00067

5. Using SYMMLQ, solve $\mathbf{M}\cdot\mathbf{x}=\mathbf{M}_0$ [Eq. (31)].

6. Construct the **B** and **C** matrices [Eqs. (25) and (26)], and finally, the **S** matrix [Eq. (24)].

7. If symmetry is used the resulting **S** matrix can be transformed back using Eqs. [(130)–(135)].

A separate program is used for each step and the intermediate results are stored on disk. This modular setup of the computation yields not only a savings in memory, but in run-time as well. For example, one can test the convergence with respect to the grid parameters, without the need to recompute the distorted waves.

A. Convergence of the unitarity of the S matrix

Four parameters specify the interaction region grid: $R^{\max}$, V^{cut}, n_θ, and the grid constant (n_B). The first two parameters determine the spacial extent and shape of the grid as discussed in Section II B. (Here we use the same $R^{\max}$ for each arrangement, although this is not strictly necessary.) n_θ is the number of Gauss–Legendre points and n_B is the number of points contained in the shortest Broglie wavelength for the two radial Jacobi coordinates (based on the total energy). In Table I we show the convergence of the unitarity of the **S** matrix as a function of n_θ and n_B, setting $R^{\max}=4.5$ Bohr and $V^{\mathrm{cut}}=3.0$ eV. As a measure of convergence we take the largest deviation from unitarity of any column of the **S** matrix in %. Below we will show to what extent this measure correlates with the error in the individual **P**-matrix elements, where $\mathbf{P}=\mathbf{S}^\dagger\cdot\mathbf{S}$. All these calculations were based on the same distorted waves (set A in Table II).

From Table I we see that the unitarity measure gives a useful first impression of the convergence of the grid. However, for large grids the deviation from unitarity can be

TABLE II. Distorted wave parameters. $R^{\max}$ (in Bohr) determines the size of the interaction region, the Numerov propagation is done outward to R' (Bohr) and all closed channels up to $E^{\max}$ (eV) are included and the column labeled n_B gives the number of points per shortest Broglie wavelength. The barrier potentials are determined by the parameters $R^{\max}$, a_1 and a_2 (in atomic units) as shown in Eq. (94).

Set	$R^{\max}$	R'	$E^{\max}$	n_B	a_1	a_2
A	4.50	15	3.0	40	0.20	0.22
B	4.75	20	3.5	60	0.10	0.11

TABLE III. Relative errors (in %) for reactive P-matrix elements.

n_B	n_θ	[a]	10^{-1}[b]	10^{-2}	10^{-3}	10^{-4}	10^{-5}
3.0	18	2.9	6.9	31	110	210	210
3.0	22	4.9(−1)[c]	1.9	11	20	56	74
3.0	26	1.1(−1)	2.0	3.4	19	41	73
3.5	26	3.1(−2)	0.12	0.89	3.7	3.7	4.0
3.5	28	4.4(−3)	0.09	0.92	3.4	3.5	4.9
4.0	28	4.8(−3)	0.13	2.1	4.1	4.5	11
4.5	28	3.6(−3)	0.44	1.9	2.0	2.2	3.3
4.5	30	1.1(−3)	0.37	1.9	2.2	2.3	2.8
4.5	32	−6.7(−4)	0.38	1.9	2.0	2.1	3.0
5.0	32	3.6(−3)	0.16	1.4	3.5	3.9	8.5
Improved distorted waves[d]							
4.5	36	2.4(−4)	0.06	0.26	0.55	0.73	1.2
4.75	36	1.8(−4)	0.20	0.71	3.3	5.8	7.5
5.0	36	8.1(−3)	0.13	0.32	5.0	5.0	11
5.5	36	1.8(−4)	0[e]	0	0	0	0
Zhang *et al.*			0.95	8.1	26	98	101

[a]The unitarity-error as in Table I.
[b]Largest relative error for all P-matrix elements larger than this.
[c]4.9(−1) denotes 4.9×10^{-1}, etc.
[d]Set B of Table II.
[e]By definition.

TABLE IV. Like Table III, but ignoring row and column 6 and 7 of the P matrix.

n_B	n_θ	10^{-1}	10^{-2}	10^{-3}	10^{-4}	10^{-5}
3.0	18	6.9	31	110	210	210
3.0	22	1.9	11	20	56	56
3.0	26	2.0	3.4	9.7	41	41
3.5	26	0.12	0.89	2.5	2.5	2.5
3.5	28	0.09	0.92	1.6	3.3	3.3
4.0	28	0.13	2.1	2.4	2.6	3.7
4.5	28	0.44	1.9	1.9	2.2	2.2
4.5	30	0.37	1.9	1.9	1.9	1.9
4.5	32	0.38	1.9	1.9	1.9	1.9
5.0	32	0.16	1.4	1.6	1.7	3.1
Improved distorted waves						
4.5	36	0.06	0.26	0.55	0.73	1.2
4.75	36	0.20	0.71	1.5	1.6	1.8
5.0	36	0.13	0.32	0.54	0.68	1.1
Zhang *et al.*		0.95	8.1	26	28	50

both positive and negative, suggesting that it can be accidentally zero without the individual P-matrix elements being exact.

B. Convergence of the individual P-matrix elements

Zhang *et al.* give the full P matrix for reaction (150) at 0.9 eV,[27] and they state: "The individual probabilities that are greater than 1.0×10^{-5} appear to be converged to about 8% or better with respect to small changes in the numerical parameters." However, for a few elements smaller than 10^{-3} we found differences with our best converged results of a factor of about 2 to 3. It turns out that these largest differences all involve the $v=1$ channels of arrangement 1; channel 6 ($v=1$, $j=0$, $\epsilon_6=0.786$ eV) and channel 7 ($v=1$, $j=2$, $\epsilon_7=0.828$ eV). Therefore, we made comparisons with and without ignoring row and column 6 and 7 of the P matrix. Also, we compared the reactive and the nonreactive matrix elements separately.

In Table III we show the relative errors in the reactive P-matrix elements, comparing to the largest calculation in the series, which has $n_B=5.5$, $n_\theta=36$, $V^{\rm cut}=3.5$ eV, $R^{\rm max}=4.75$ Bohr and is based on improved distorted waves (set B in Table II). We show the largest relative error for all reactive elements larger than $10^{-1},10^{-2},\ldots,10^{-5}$. The first 8 entries in the table are based on the distorted waves set A (Table II and $V^{\rm cut}=3.0$ eV) and the next three entries are based on the improved distorted waves (set B, $V^{\rm cut}=3.5$ eV) where the errors of the calculation with $n_B=5.5$ are set to zero by definition. A careful inspection of this table shows that when the unitarity error is less than, say, 0.1% it no longer correlates with the errors in the individual P-matrix elements. Furthermore, for the elements greater than 10^{-2} the convergence is better than 2% and the agreement with the results of Zhang *et al.* (the last entry in the table) is very good. For the smaller elements there are variations on the order of 10% but some elements differ from Zhang's results by up to a factor of two.

In Table IV we show the same calculations, but we ignore rows and columns 6 and 7 in the comparison. This table clearly shows much better convergence. Also the agreement with Zhang's results for the small P-matrix elements is improved, although the differences are still larger than the 8% Zhang *et al.* suggested.

Although the reactive elements are the primary interest of this work, we do think it is instructive to show the convergence tests for the nonreactive elements. In Table V the results for arrangement 1 are shown, and Table VI shows again the effect of ignoring the $v=1$ channels. The behavior is similar to what we saw for the reactive elements, but the effect of ignoring the $v=1$ channels is even more dramatic. Apart from this, we also want to draw attention to the fact that the first three entries in those two tables suggest that in order to converge the arrangement 1 inelastic elements we do not need very many θ points. In Table VII we show that quite the opposite is true for arrangement 2 (and 3). This should not be too surprising,

TABLE V. Like Table III, for the inelastic elements of arrangement 1.

n_B	n_θ	10^{-1}	10^{-2}	10^{-3}	10^{-4}	10^{-5}
3.0	18	6.1	6.5	6.5	93	93
3.0	22	6.1	6.5	6.5	93	93
3.0	26	6.0	6.5	6.5	93	93
3.5	26	0.42	0.55	0.55	4.6	4.6
3.5	28	0.44	0.96	0.96	4.6	4.6
4.0	28	0.41	0.63	0.63	25	25
4.5	28	1.2	1.2	1.24	5.6	5.6
4.5	30	1.1	1.1	1.1	5.8	5.8
4.5	32	1.1	1.2	1.2	5.6	5.6
5.0	32	0.33	0.49	0.49	20	20
Improved distorted waves						
4.5	36	0.09	0.09	0.09	1.2	1.2
4.75	36	0.38	0.87	0.87	20	20
5.0	36	0.27	0.77	0.77	12	12
Zhang *et al.*		7.4	33	33	98	360

TABLE VI. Like Table V, but ignoring row and column 6 and 7 of the P matrix.

n_B	n_θ	10^{-1}	10^{-2}	10^{-3}	10^{-4}	10^{-5}
3.0	18	6.1	6.4	6.4	6.4	6.4
3.0	22	6.1	6.1	6.1	6.1	6.1
3.0	26	6.0	6.0	6.0	6.0	6.0
3.5	26	0.42	0.55	0.55	0.55	0.55
3.5	28	0.44	0.96	0.96	0.96	0.96
4.0	28	0.41	0.41	0.41	0.41	0.41
4.5	28	1.2	1.2	1.2	1.2	1.2
4.5	30	1.0	1.1	1.1	1.1	1.1
4.5	32	1.1	1.2	1.2	1.2	1.2
5.0	32	0.33	0.45	0.45	0.45	0.45
Improved distorted waves						
4.5	36	0.09	0.09	0.09	0.09	0.10
4.75	36	0.38	0.87	0.87	0.87	0.87
5.0	36	0.27	0.32	0.32	0.32	0.32
Zhang *et al.*		7.4	7.4	26	26	26

since for the interaction region grid Jacobi coordinates of arrangement 1 are being used.

As a last convergence test we show the effect of the cutoff energy V^{cut} in Table VIII. The table shows that V^{cut} becomes the limiting factor when it is less than, roughly, 3 eV. The same pattern is repeated for the nonreactive elements.

Regarding the discrepancies with Zhang's results for the smaller probabilities, if it is our results that are inaccurate, a possible explanation could lie in our omission of closed distorted waves in the free basis (see the discussion at the end of Section II B). Although we checked convergence with respect to $R^{\max}$, some barely closed channels might demand even larger grids and it might be better to explicitly include closed distorted waves. We are currently investigation this possibility.

C. Distorted waves

In Figure 1 we show a two-dimensional cut through the PES at $\theta=0$ (i.e., the collinear configuration). The dots are the grid points for $n_B=3.5$, $R^{\max}=4.5$ Bohr, and

TABLE VII. Like Table III, for the inelastic elements of arrangement 2 (and 3).

n_B	n_θ	10^{-1}	10^{-2}	10^{-3}	10^{-4}	10^{-5}
3.0	18	79	155	1400	6200	69000
3.0	22	24	35	56	280	2900
3.0	26	5.4	8.5	31	150	420
3.5	26	4.6	4.7	12	42	74
3.5	28	1.9	3.6	7.9	16	27
4.0	28	0.98	2.8	9.3	14	32
4.5	28	3.1	4.5	7.8	14	31
4.5	30	1.7	4.4	4.4	6.8	9.7
4.5	32	1.3	2.8	4.9	8.6	8.6
5.0	32	0.69	1.9	6.8	10	10
Improved distorted waves						
4.5	36	0.68	0.72	1.2	1.8	2.1
4.75	36	0.98	0.98	1.5	4.7	4.7
5.0	36	1.3	1.3	2.5	2.5	3.4

TABLE VIII. The effect of V^{cut} on the relative errors in the reactive elements P matrix elements. Here we use $n_\theta=28$ and $n_B=3.5$.

V^{cut}		10^{-1}	10^{-2}	10^{-3}	10^{-4}	10^{-5}
2.0	0.66	0.88	12	43	44	86
2.5	0.007	0.83	5.7	15	15	21
3.0	0.0044	0.09	0.92	3.4	3.5	4.9
3.5	0.0044	0.13	0.98	2.8	3.3	4.4

$V^{\text{cut}}=3.5$ eV. In arrangement 1 ($R>r$) we show a contour plot of the real part of $(\hat{H}-E)\chi_{v=0,j=0}$ [see Eq. (62)] for an undistorted wave and in arrangement 2 ($R<r$) the same quantity for a distorted wave. The undistorted wave is a Hankel function [Eq. (17)] times a cutoff function

$$f(R)=(e^{-A/R})^n \tag{151}$$

with $A=4.0$ Bohr and $n=14$. The distorted wave parameters correspond to set A of Table II. The figure clearly shows that for the distorted wave, $(\hat{H}-E)\chi$ lies completely within the grid with $R^{\max}=4.5$ Bohr, while for the undistorted wave, $(\hat{H}-E)\chi$ extends to approximately 5.5 Bohr. Note that for the distorted waves $(\hat{H}-E)\chi$ must be zero outside the grid by construction, while for the undistorted waves it will formally be zero only in the asymptotic region where $\Delta V_\alpha(R_\alpha,r_\alpha,z_\alpha)=0$. In the three-dimensional grid the number of grid points scales with the square of $R^{\max}$. In the current example, taking $n_\theta=28$, we have $n=4964$ points for $R^{\max}=4.5$ Bohr and $n=6943$ for $R^{\max}=5.5$ Bohr. Furthermore, the number of angular points needed for a specified accuracy increases with $R^{\max}$ since the points laid down in Jacobi coordinates of arrangement

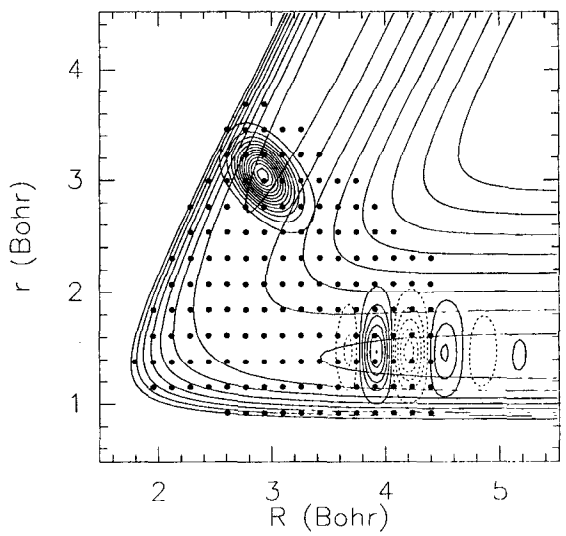

FIG. 1. Contour lines of the PES are shown for 0.2,0.6,1.0,...,3.0 eV at $\theta=0$. In arrangement 1 ($R>r$) we show a contour plot of the real part of $(\hat{H}-E)\chi_{j=0,v=0}$ for an undistorted wave (equidistant, arbitrary units, solid lines positive, dashed lines negative) and in arrangement 2 ($R<r$) we show a the corresponding plot for a distorted wave. The dots represent the grid points.

1 spread out in arrangements 2 and 3. Below we shall see that the CPU-time scales roughly with N^2 showing the importance of the use of distorted waves.

D. Timings

We report timings for the solution of a single complex right hand side of Eq. (31) using the SYMMLQ algorithm (see Section III), since solving the linear system is the most time-consuming part of the Kohn calculation (the costs are about the same for each rhs). (Actually, in the current examples the construction of the distorted waves can be about as expensive as the inversion step, since we have not yet fully optimized the parameters in the renormalized Numerov calculation. Also, note that a wave-function-following method like the renormalized Numerov method cannot be expected to be the most efficient algorithm to treat the long range part of the potential. All the other steps together take less than a few % of the total cpu-time.) The SYMMLQ algorithm is an iterative method and it must be run separately for each right-hand side. Actually, since the columns of $\mathbf{M}_0$ are complex, SYMMLQ must be run twice for each open channel. The cost of each run is almost exactly equal to the cost of a sparse matrix-vector multiplication times the number of iterations. As an example we take a calculation with $n_B=3.5$, $n_\theta=26$, $V^{\rm cut}=3.0$ eV, and $R^{\rm max}=4.5$ Bohr. The resulting number of grid points is $N=4599$, using symmetry. There are 24 open channels and the cpu-time per open channel (i.e., to run SYMMLQ twice) is 56 seconds on an IBM RS6000/580 workstation. The number of iterations needed to converge the linear system to a residual of length 10^{-4} (10^{-7}) is about 1100 (1400). The number of floating point operations needed for one matrix-vector multiplication is about 4.1×10^5, corresponding to an average of 45 nonzero matrix elements per row. The estimated number of floating point operations per second (counting both additions and multiplications) is somewhat above 25×10^6 (please use this figure only as a rough indication).

For all the calculations in Table I we have plotted the cpu-time (t) vs the number of grid points (N) and it turns out that the CPU-time scales as $t\sim N^2$. This scaling cannot be derived from a simple operation count (due to the unpatterned sparse matrix structure), but is the combined effect of the increase of the number of iterations and the higher cost per iteration with increasing N.

Finally, in Tables IX and X we give a few more examples of how the number of grid points, the number of iterations and the CPU-time per open channel depend on the grid parameters. Note that the relative number of iterations ($n_{\rm iter}/N$) is the largest for the low-quality grids. The last column in these two tables shows that the CPU-times scales roughly with N^2.

TABLE IX. A few examples of how the number of grid points (N), the number of iterations needed to obtain a residual error of 10^{-7}, and the CPU-time per open channel (t) depend on the grid parameters. In all these examples we have $R^{\rm max}=4.5$ Bohr and $V^{\rm cut}=3.0$ ($n_{\rm iter}$ and t are rounded to two significant figures).

n_B	n_θ	N	$n_{\rm iter}$	t	$n_{\rm iter}/N$	t/N^2
3.0	18	2291	1100	20	0.49	9.2
3.0	22	2797	1300	29	0.46	8.8
3.0	26	3305	1500	40	0.46	8.9
3.5	26	4599	1400	56	0.31	6.4
3.5	28	4964	1500	69	0.31	6.8
4.0	28	6428	2600	160	0.40	9.1
4.5	28	8202	2100	180	0.26	6.3
4.5	30	8780	2300	210	0.26	6.6
4.5	32	9364	2500	260	0.27	7.2
5.0	32	11532	3400	410	0.29	7.3

VIII. CONCLUSION AND FUTURE WORK

The main bottleneck for variational quantum reactive scattering calculations for larger systems or at higher energies is the storage requirement for the interaction-region Hamiltonian matrix. We have demonstrated that this memory problem can be solved by using a discrete representation, resulting in a sparse Hamiltonian matrix. The sparsity is further exploited by using an iterative method to solve the resulting linear equations. The key to the application of a discrete representation is the use of a single interaction region coordinate system. This represents an essential departure from Miller's approach[10] of using a multicentered expansion of the wave function. The price one pays is that the representation will typically be less efficient than one based on a multicentered expansion of the wave function.

We have shown how the number of grid points can be reduced by truncating the grid and by the use of distorted waves, in order to speed up the calculation. Our construction of distorted waves makes a clean distinction between the "interaction region" and the "asymptotic region", thus removing the size of the interaction region as a convergence parameter.

A disadvantage of an iterative method for solving linear equations, compared to, e.g., LU-decomposition, is that the cpu-time scales linearly with the number of right-hand sides. In work we are pursuing on the $H+O_2$ system we found that it is possible to eliminate from the open channel space linear combinations that barely reach the interaction region, thus reducing the number of rhs. [Those linear combinations are the ones that do not "feel" the difference between the two barrier potentials and thus cause Δ [Eq. (79)] to become nearly singular. Thus, eliminating them also solves this singularity problem.] Furthermore, if one manages to develop a method for computing one column of the S matrix based on solving only one set of linear equations, this iterative method will be very competitive compared to direct methods (see also Refs. 7, 29, and 30). It

TABLE X. Like Table IX, but with $n_\theta=28$ and $n_B=3.5$.

$V^{\rm cut}$	N	$n_{\rm iter}$	t	$n_{\rm iter}/N$	t/N^2
2.0	3691	2000	59	0.54	10
2.5	4400	2400	88	0.55	11
3.0	4964	1600	69	0.31	6.8
3.5	5367	2000	91	0.36	7.6

might also be interesting to note that calculations for several rhs can easily be run in coarse grained parallel. Our code has been made suitable for this and we have already done some calculations on HO_2 spread over four workstations located on two different continents.

With the present method one has the freedom to use all kinds of interaction region coordinates. In this paper we present an example employing the Jacobi coordinates of one arrangement. We also employed other coordinate systems like valence (bond-angle) coordinates and Radau coordinates.[13] The valence coordinates give a slightly better representation for the reactions we have studied, but the since the kinetic energy operator has more terms here than for orthogonal coordinates, there was no reduction in overall cost of the calculation. It might be interesting to try hyperspherical coordinates, since they have been used as global coordinates for reactive systems before.[31] An advantage of these coordinates is that they allow the use of the full symmetry in systems with three-fold symmetry (like H_3).

It might be possible to speed up the matrix-vector multiplication by employing other (discrete) representations. For example, one could use fast Fourier transform techniques such as those being used in time-dependent calculations.[32] Also, finite-order finite difference representations of the kinetic energy could be used, giving rise to kinetic energy matrices with finite bandwidth. Also the use of so-called distributed approximating functions (DAFs)[33] gives rise to banded kinetic energy matrices.

We conclude that we have presented a viable method, with minimal memory requirements, employing several techniques to reduce the computational effort, while routes for further improvements have been indicated.

ACKNOWLEDGMENTS

The authors wish to thank Professor W. H. Miller for his enthusiastic support and guidance of this work. We thank Scott M. Auerbach for many very useful and enlightening discussions. We also thank Professor A. van der Avoird for critically reading the manuscript. This work was supported by the National Science Foundation, Grant No. CHE 89-20690. G.C.G also acknowledges support from the Eindhoven University of Technology, the Netherlands Organization for Scientific Research (NWO) and the Royal Netherlands Academy of Arts and Sciences (KNAW).

APPENDIX A: PROJECTION TECHNIQUE

Here we describe the projection technique used to reduce the number of iterations (see Section III). For certain values of (i) and (j) it might happen that none of the points $\{(R_i,r_j,z_k),\ k=1,\ldots,n_\theta\}$ are being eliminated by the potential energy criterion ($V^{\rm cut}$). In particular, this can be expected to occur for small R_i. In those cases, the angular DVR can be transformed back to the Gauss–Legendre basis ($\bar{P}_j, j=0,\ldots,n_\theta-1$). The (1D) kinetic energy of function $\bar{P}_j$ is given by

$$T_j=\left(\frac{1}{2\mu R_i^2}+\frac{1}{2mr_j^2}\right)j(j+1). \tag{A1}$$

The idea of the projection technique is to remove the functions $\bar{P}_j$ for which $T_j > V^{\rm cut}$ and transform back to point-space. This must be done before and after the matrix-vector multiplication, i.e., twice for each iteration. The projection is also applied to the right-hand side [Eq. (31)]. This way we can work in the projected space without the need to modify the subroutine for the matrix vector multiplication.

APPENDIX B: DERIVATION OF THE INTERPOLATION FORMULA

Here we derive the interpolation formula Eq. (90). From Eqs. (88) and (89) we have

$$R_a=R_{i-1}+ah=R_i-bh \tag{B1}$$

with $a+b=1$. We can now write Taylor expansions about R_{i-1} and about R_i

$$U(R_a)=U_{i-1}+(ah)U'_{i-1}+\frac{(ah)^2}{2}U''_{i-1}+\frac{(ah)^3}{6}U'''_{i-1}+O(h^4), \tag{B2}$$

$$U(R_a)=U_i-(bh)U'_i+\frac{(bh)^2}{2}U''_i-\frac{(bh)^3}{6}U'''_i+O(h^4). \tag{B3}$$

Multiplying Eq. (B2) by b and Eq. (B3) by a and adding them gives

$$U(R_a)=bU_{i-1}+aU_i+abh(U'_{i-1}-U'_i)+\frac{abh^2}{2}[aU''_{i-1}+bU''_i]+\frac{abh^3}{6}[a^2U'''_{i-1}-b^2U'''_i]+O(h^4). \tag{B4}$$

To eliminate the first derivatives in this expression we start with yet another Taylor expansion

$$U_i=U_{i-1}+hU'_{i-1}+\frac{h^2}{2}U''_{i-1}+O(h^3), \tag{B5}$$

and take its derivative and multiply by h to get

$$h(U'_i-U'_{i-1})=h^2U''_{i-1}+\frac{h^3}{2}+O(h^4). \tag{B6}$$

For the second derivative terms we use [cf. Eq. (69)]

$$U''_j=W_jU_j \tag{B7}$$

and for the third derivative terms we have

$$U'''_{i-1}=U'''_i+O(h^4)=\frac{U''_i-U''_{i-1}}{h}+O(h^4). \tag{B8}$$

Substituting Eqs. (B6), (B7), and (B8) into Eq. (B4) gives the final fourth-order interpolation formula Eq. (90).

[1] W. H. Miller and B. M. D. D. Jansen op de Haar, J. Chem. Phys. **86**, 6213 (1987).
[2] J. Z. H. Zhang, S.-I. Chu, and W. H. Miller, J. Chem. Phys. **88**, 6233 (1988); **89**, 4454 (1988).
[3] J. Z. H. Zhang and W. H. Miller, J. Chem. Phys. **88**, 4549 (1988).
[4] J. Z. H. Zhang and W. H. Miller, J. Chem. Phys. **91**, 1528 (1989).
[5] J. Z. H. Zhang and W. H. Miller, J. Phys. Chem. **94**, 7785 (1990).
[6] D. C. Chatfield, R. S. Friedman, G. C. Lynch, D. G. Truhlar, and D. W. Schwenke, J. Chem. Phys. **98**, 342 (1993), and references therein.
[7] D. E. Manolopoulos, M. D'Mello, and R. E. Wyatt, J. Chem. Phys. **91**, 6096 (1989).
[8] G. H. Golub and C. F. van Loan, *Matrix Computations*, 2nd ed. (Johns Hopkins University Press, Baltimore, Maryland, 1989), Chap. 3.
[9] D. T. Colbert and W. H. Miller, J. Chem. Phys. **96**, 1982 (1992).
[10] W. H. Miller, J. Chem. Phys. **50**, 407 (1969).
[11] M. Abramowitz and I. A. Stegun, *Handbook of Mathematical Functions* (U.S. Government Printing Office, Washington, D.C., 1964), Number 10.1.1, p. 437.
[12] See Ref. 11, Number 22.2, p. 775.
[13] B. R. Johnson and W. P. Reinhardt, J. Chem. Phys. **85**, 4538 (1986).
[14] J. T. Muckerman, Chem. Phys. Lett. **173**, 200 (1990).
[15] D. T. Colbert and W. H. Miller (unpublished).
[16] C. C. Paige and M. A. Saunders, Siam J. Numer. Anal. **12**, 617 (1975).
[17] R. A. Friesner, J. A. Bentley, M. Menou, and C. Leforestier, J. Chem. Phys. **99**, 324 (1993).
[18] (a) J. V. Lill, G. A. Parker, and J. C. Light, Chem. Phys. Lett. **89**, 483 (1982); (b) J. C. Light, I. P. Hamiltonian, and J. V. Lill, J. Chem. Phys. **82**, 1400 (1985); (c) J. V. Lill, G. A. Parker, and J. C. Light, *ibid.* **85**, 900 (1986); (d) S. E. Choi and J. C. Light, *ibid.* **92**, 2129 (1990); (e) J. C. Light, R. M. Whitnell, T. J. Park, and S. E. Choi, NATO ASI Ser. C **277**, 187 (1989).
[19] D. O. Harris, G. G. Engerholm, and W. D. Gwinn, J. Chem. Phys. **43**, 1515 (1965).
[20] A. S. Dickinson and P. R. Certain, J. Chem. Phys. **49**, 4209 (1968).
[21] C. Schwartz, J. Math. Phys. **26**, 411 (1985).
[22] The NAG Fortran Library Manual, Mark 15 (The Numerical Algorithms Group Limited, Oxford, UK, 1991), routine M01DZF.
[23] Y. Shima and M. Baer, Chem. Phys. Lett. **91**, 43 (1982).
[24] Y. Shima, M. Baer, and D. J. Kouri, Chem. Phys. Lett. **94**, 321 (1983).
[25] B. R. Johnson, J. Chem. Phys. **67**, 4086 (1977).
[26] B. R. Johnson, National Resource for Computation in Chemistry, University of California, Berkeley, NRCC, Proceedings No. 5, 86 (1979).
[27] J. Z. H. Zhang, D. J. Kouri, K Haug, D. W. Schwenke, Y Shima, and D. G. Truhlar, J. Chem. Phys. **88**, 2492 (1988).
[28] P. Siegbahn and B. Liu, J. Chem. Phys. **68**, 2457 (1978); D. G. Truhlar and C. J. Horowitz, *ibid.* **68**, 2466 (1978); **71**, 1514(E) (1979).
[29] W. H. Thompson and W. H. Miller, Chem. Phys. Lett. **206**, 123 (1993).
[30] S. M. Auerbach and C. Leforestier, Comput. Phys. Commun. (in press).
[31] R. T Pack and G. A. Parker, J. Chem. Phys. **87**, 3888 (1987).
[32] R. Kosloff, J. Phys. Chem. **92**, 2087 (1988).
[33] D. K. Hoffman, N. Nayar, O. A. Sharafeddin, and D. J. Kouri, J. Phys. Chem. **95**, 8299 (1991).